Cell Reports, Volume *16*

Supplemental Information

$BRAF^{V600E}$ Kinase Domain Duplication Identified in Therapy-Refractory Melanoma Patient-Derived Xenografts

Kristel Kemper, Oscar Krijgsman, Xiangjun Kong, Paulien Cornelissen-Steijger, Aida Shahrabi, Fleur Weeber, Daphne L. van der Velden, Onno B. Bleijerveld, Thomas Kuilman, Roel J.C. Kluin, Chong Sun, Emile E. Voest, Young Seok Ju, Ton N.M. Schumacher, A.F. Maarten Altelaar, Ultan McDermott, David J. Adams, Christian U. Blank, John B. Haanen, and Daniel S. Peeper

Figure S1

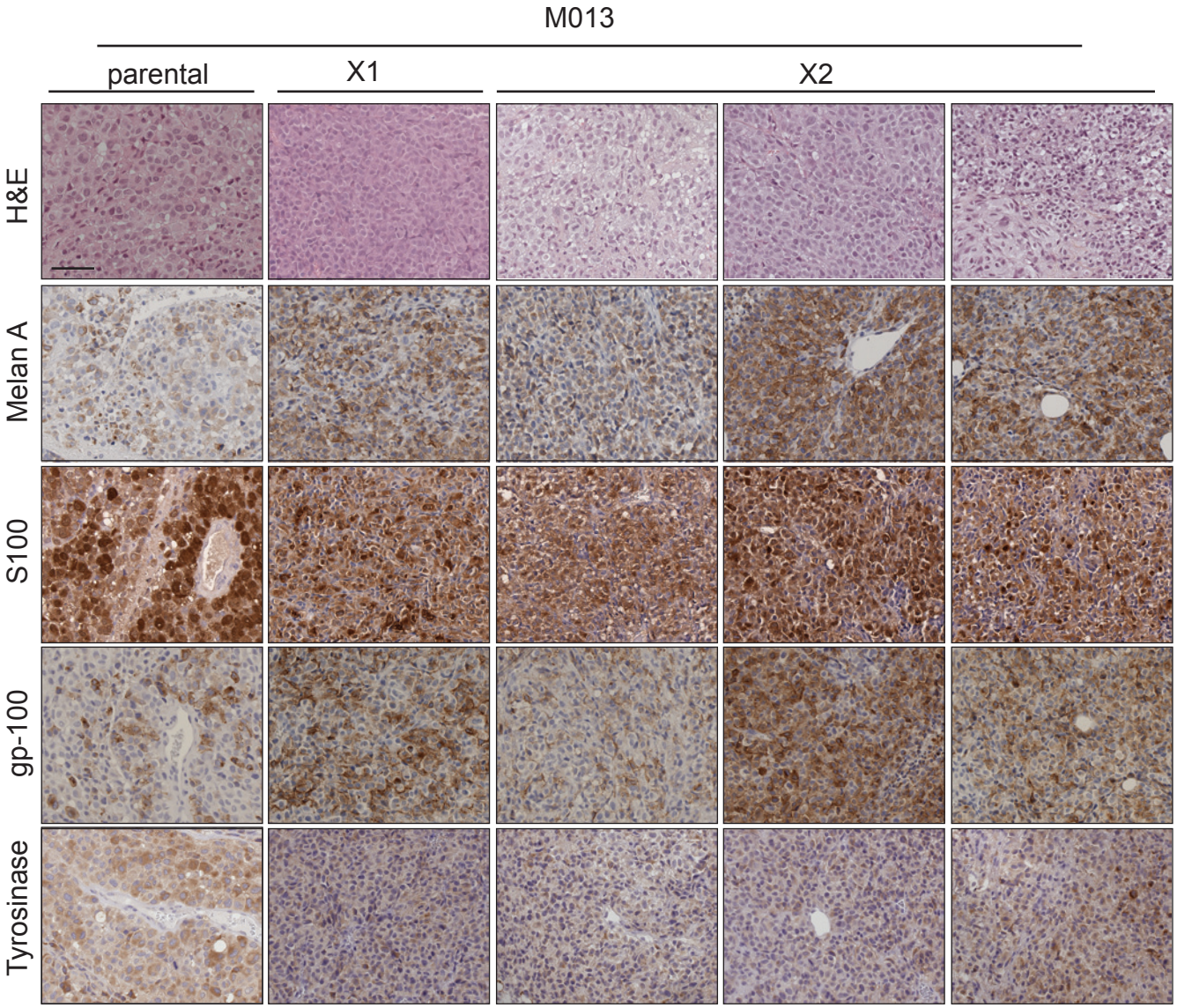

Figure S2

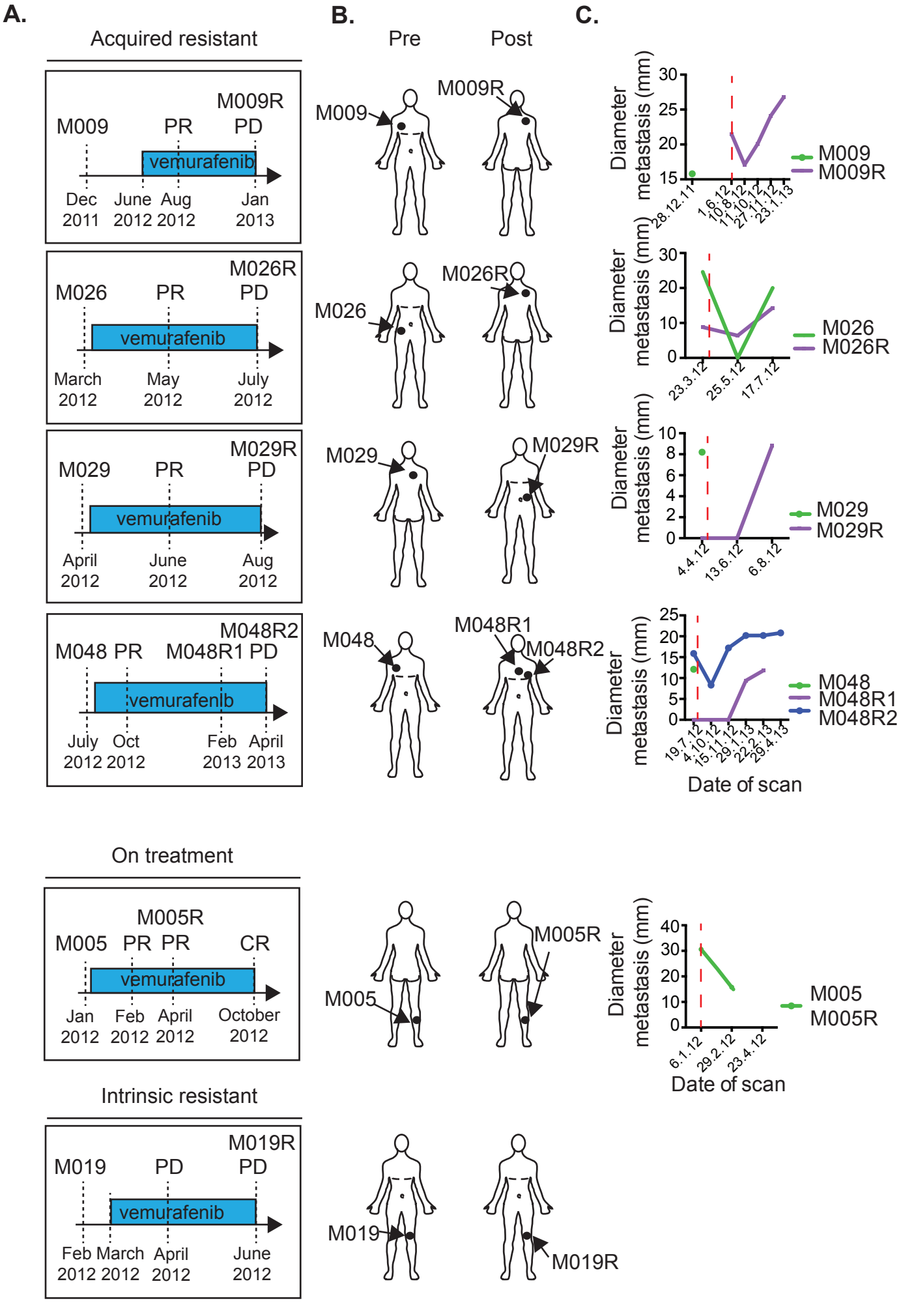
A.
B.
C.
Acquired resistant
Pre
Post
M009
PR
M009R
PD
vemurafenib
Dec 2011
June 2012
Aug 2012
Jan 2013
M026
M026R
March 2012
May 2012
July 2012
M029
M029R
April 2012
June 2012
Aug 2012
M048
PR
M048R1
PD
M048R2
July 2012
Oct 2012
Feb 2013
April 2013
Diameter metastasis (mm)
28.12.11
1.6.12
10.8.12
11.10.12
27.11.12
23.1.13
23.3.12
25.5.12
17.7.12
4.4.12
13.6.12
6.8.12
19.7.12
4.10.12
15.11.12
29.1.13
22.2.13
29.4.13
Date of scan
On treatment
M005
M005R
Jan 2012
Feb 2012
April 2012
October 2012
6.1.12
29.2.12
23.4.12
Intrinsic resistant
M019
M019R
Feb 2012
March 2012
April 2012
June 2012

Figure S3

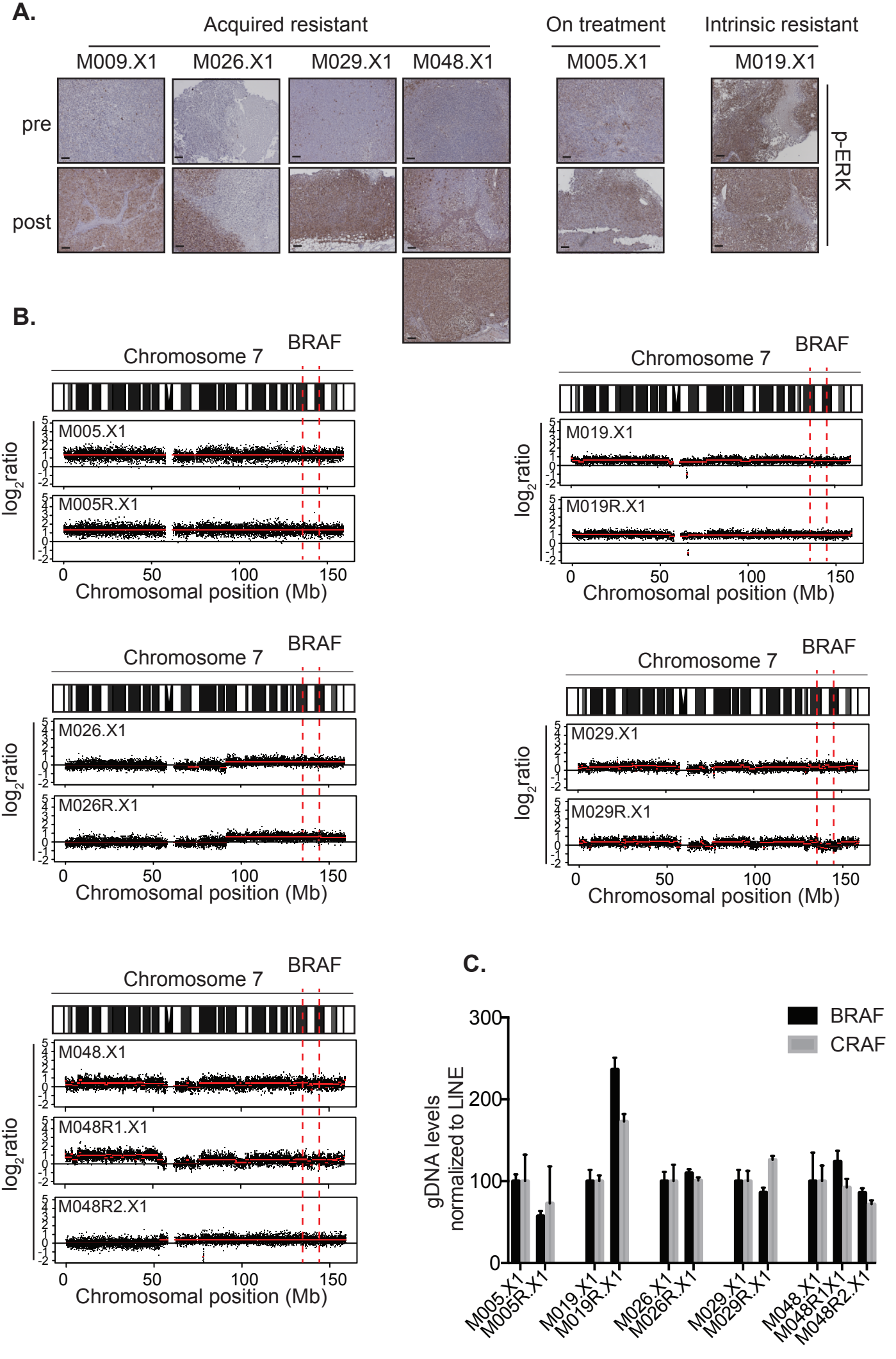
A.
Acquired resistant
On treatment
Intrinsic resistant
M009.X1
M026.X1
M029.X1
M048.X1
M005.X1
M019.X1
pre
post
p-ERK
B.
Chromosome 7
BRAF
M005.X1
M005R.X1
M019.X1
M019R.X1
M026.X1
M026R.X1
M029.X1
M029R.X1
M048.X1
M048R1.X1
M048R2.X1
log2ratio
Chromosomal position (Mb)
C.
gDNA levels normalized to LINE
BRAF
CRAF
M005.X1
M005R.X1
M019.X1
M019R.X1
M026.X1
M026R.X1
M029.X1
M029R.X1
M048.X1
M048R1X1
M048R2.X1

Figure S4

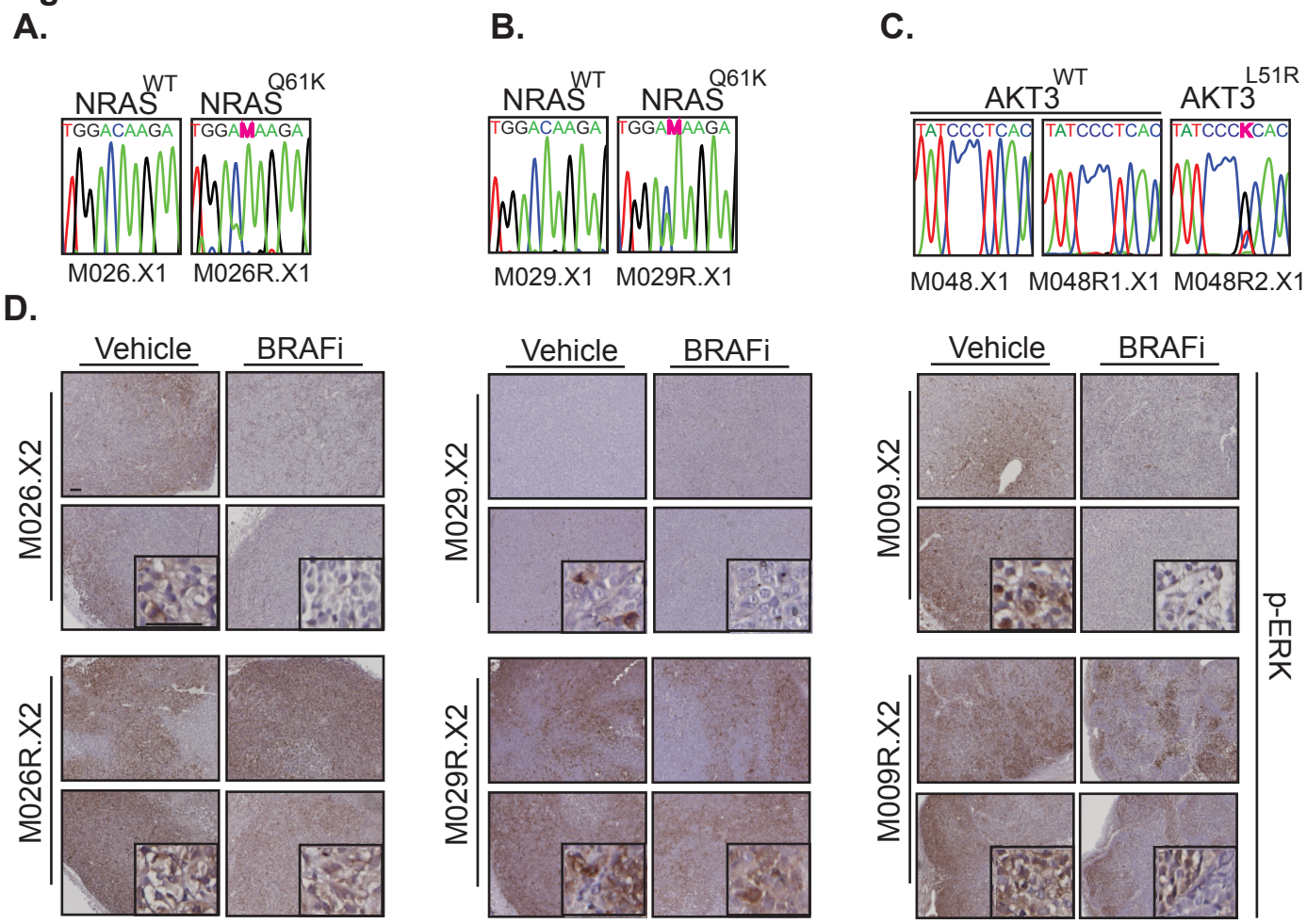
A.
NRAS WT
NRAS Q61K
TGGACAAGA
TGGAMAAGA
M026.X1
M026R.X1
B.
NRAS WT
NRAS Q61K
TGGACAAGA
TGGAMAAGA
M029.X1
M029R.X1
C.
AKT3 WT
AKT3 L51R
TATCCCTCAC
TATCCCTCAC
TATCCCKCAC
M048.X1
M048R1.X1
M048R2.X1
D.
Vehicle
BRAFi
M026.X2
M026R.X2
M029.X2
M029R.X2
M009.X2
M009R.X2
p-ERK

Figure S5

A.

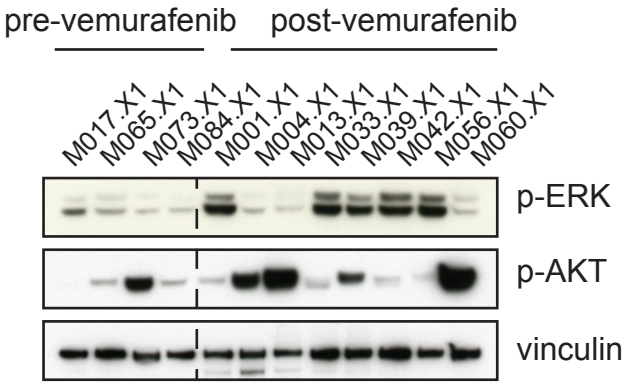
pre-vemurafenib
post-vemurafenib
M017.X1
M065.X1
M073.X1
M084.X1
M001.X1
M004.X1
M013.X1
M033.X1
M039.X1
M042.X1
M056.X1
M060.X1
p-ERK
p-AKT
vinculin

B.

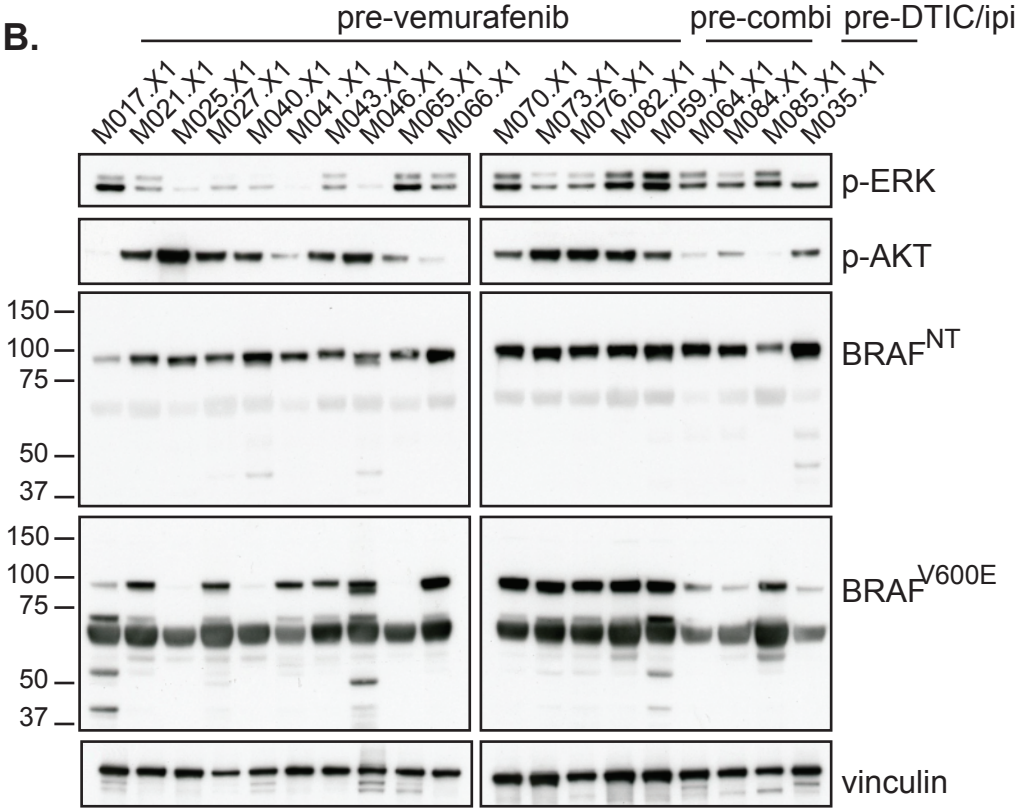
pre-vemurafenib
pre-combi
pre-DTIC/ipi
M017.X1
M021.X1
M025.X1
M027.X1
M040.X1
M041.X1
M043.X1
M046.X1
M065.X1
M066.X1
M070.X1
M073.X1
M076.X1
M082.X1
M059.X1
M064.X1
M084.X1
M085.X1
M035.X1
p-ERK
p-AKT
150
100
75
50
37
BRAF^NT
150
100
75
50
37
BRAF^V600E
vinculin

Figure S6

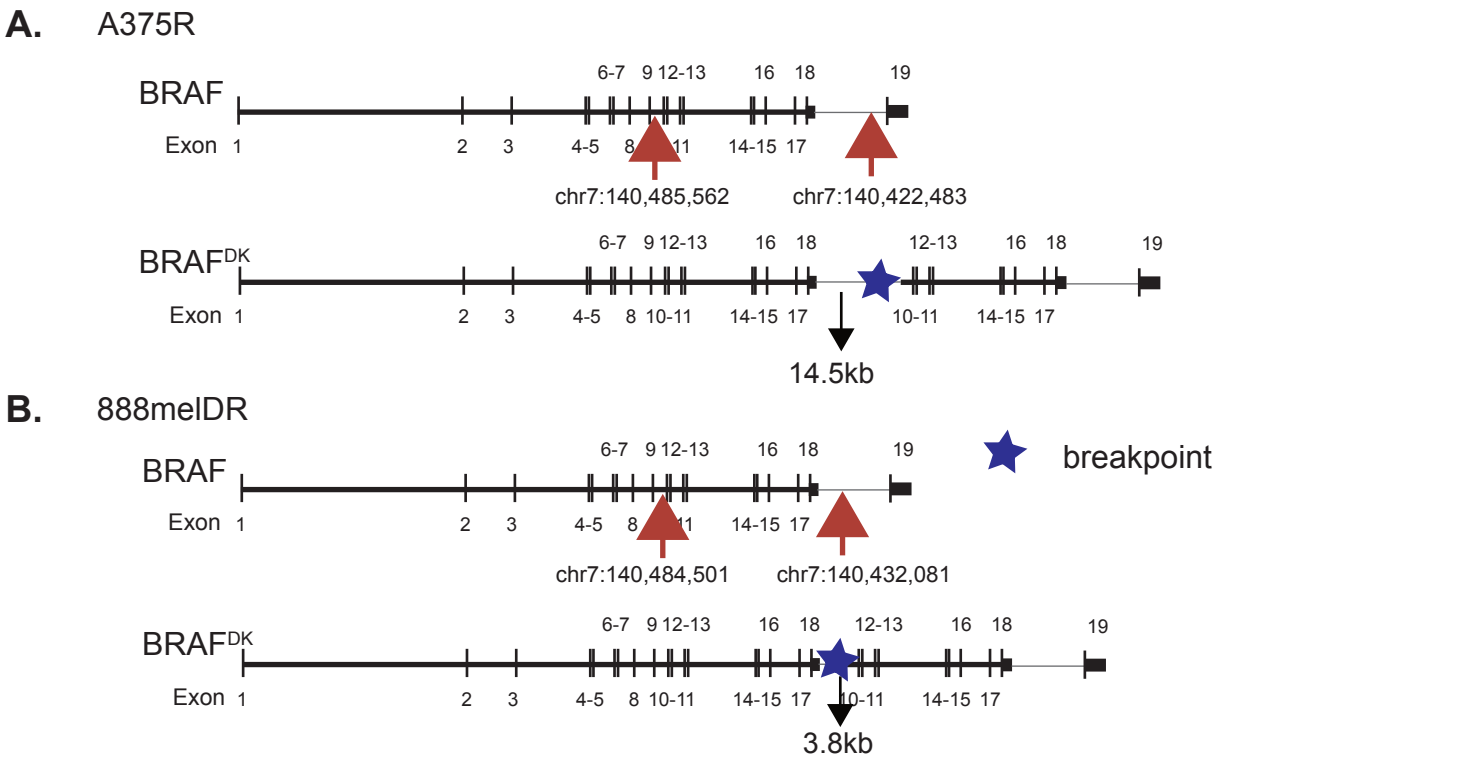
A.
A375R
BRAF
Exon 1 2 3 4-5 8 11 14-15 17
6-7 9 12-13 16 18 19
chr7:140,485,562
chr7:140,422,483
BRAFDK
Exon 1 2 3 4-5 8 10-11 14-15 17 10-11 14-15 17
6-7 9 12-13 16 18 12-13 16 18 19
14.5kb
B.
888melDR
BRAF
Exon 1 2 3 4-5 8 11 14-15 17
6-7 9 12-13 16 18 19
breakpoint
chr7:140,484,501
chr7:140,432,081
BRAFDK
Exon 1 2 3 4-5 8 10-11 14-15 17 10-11 14-15 17
6-7 9 12-13 16 18 12-13 16 18 19
3.8kb

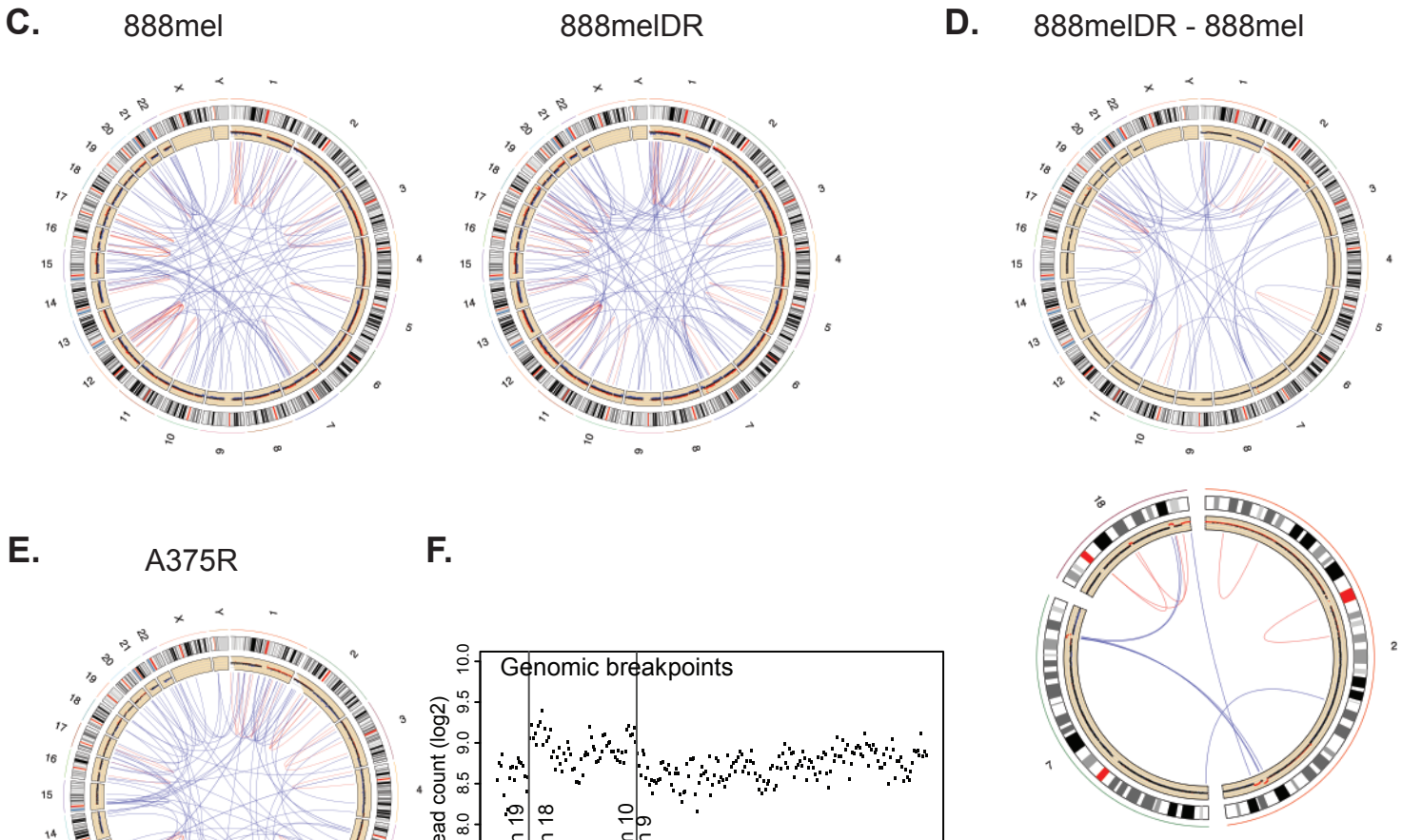
C.
888mel
888melDR
D.
888melDR - 888mel

E.
A375R
F.
Genomic breakpoints
Read count (log2)
7.0 7.5 8.0 8.5 9.0 9.5 10.0
exon 19
exon 18
exon 10
exon 9
BRAF
140.4 140.5 140.6
Genomic location (Mb)

Figure S7

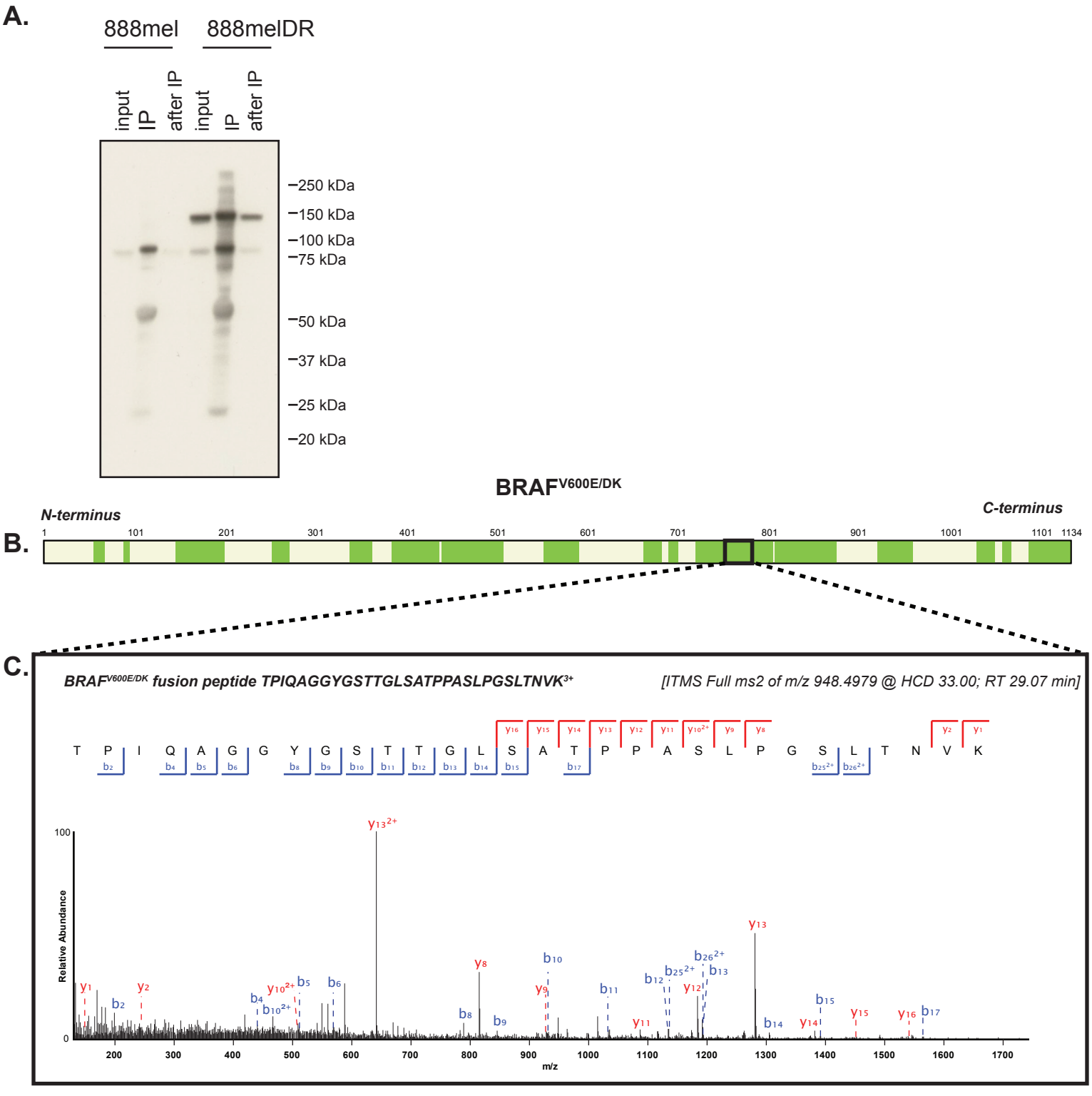
A.
888mel
888melDR
input
IP
after IP
input
IP
after IP
250 kDa
150 kDa
100 kDa
75 kDa
50 kDa
37 kDa
25 kDa
20 kDa
B.
BRAF V600E/DK
N-terminus
C-terminus
1
101
201
301
401
501
601
701
801
901
1001
1101
1134
C.
BRAF V600E/DK fusion peptide TPIQAGGYGSTTGLSATPPASLPGSLTNVK 3+
[ITMS Full ms2 of m/z 948.4979 @ HCD 33.00; RT 29.07 min]
T P I Q A G G Y G S T T G L S A T P P A S L P G S L T N V K
Relative Abundance
m/z
100
0
200
300
400
500
600
700
800
900
1000
1100
1200
1300
1400
1500
1600
1700

Supplemental Figure legends:

Figure S1. Stable marker expression upon *in vivo* passaging of melanoma PDX, Related to Figure 1.
H&E stainings and IHC stainings for MelanA, S100, gp-100 and tyrosinase were performed on the parental tumor and two subsequent passages of PDX (X1 and X2). Scale bars indicate 100 μm.

Figure S2. Clinical histories of patients from matched pre- and post-vemurafenib PDX pairs, Related to Figure 2.
A. Vemurafenib treatment schedule for each patient from whom we obtained tumor specimens before start of treatment, during treatment or after resistance had occurred. Indicated are the time points when the samples were taken. The overall response, according to RECIST 1.1 criteria, is indicated. **B.** Location of each of the obtained patient samples. **C.** For each individual lesion, the diameter was measured at baseline (before start of treatment) and every two consecutive months during treatment until progressive disease was observed. For one patient (M019), the CT-scans of the tumor location were unavailable. Vertical dashed line indicates start of vemurafenib treatment. For three patients (M009, M029, M048), the pre-treatment PDX were derived from lesions that were surgically removed before the start of treatment and these tumors did not recur at those particular locations. One pre-treatment PDX was derived from a lesion that showed a complete response (CR) to vemurafenib before it recurred (M026) According to the response data, we have grouped these PDX pairs in 1) acquired resistant 2) on treatment and 3) intrinsic resistant.

Figure S3. BRAF amplification was not detected in the other matched PDX pairs, Related to Figure 2.
A. Staining for p-ERK on FFPE archival material of the matched PDX pairs. Scale bars indicate 100 μm. **B.** No amplification of the genomic region containing BRAF was identified in any of the matched PDX pairs. Only M019R.X1 showed a complete duplication of chromosome 7. **C.** Validation of the absence of the *BRAF* amplification was performed by qPCR on genomic. *CRAF* was included as a negative control. CT values were normalized to *LINE*. Error bars indicate standard deviation.

Figure S4. Validation of the mechanisms and the resistance in PDX, Related to Figure 2 and 3.
A. Validation of $NRAS^{Q61K}$ ($NRAS^{C181A}$) mutation in M026R.X1 and **B.** M029R.X1 by Sanger sequencing. **C.** Validation of $AKT3^{L51R}$ ($AKT3^{T152G}$) mutation in M048R2.X1 by Sanger sequencing. **D.** Staining for p-ERK on FFPE material of the matched PDX pairs M026/R.X2, M029/R.X2 and M009/R.X2 treated with vehicle or 30 mg/kg dabrafenib. Scale bars indicate 100 μm.

Figure S5. Analysis of a panel of pre-treatment PDX for presence of $BRAF^{V600E/DK}$, Related to Figure 5.
Immunoblotting to detect the presence of $BRAF^{V600E/DK}$ in a panel of pre-treatment PDX, using two different antibodies, recognizing either a N-terminal epitope ($BRAF^{NT}$) or the $BRAF^{V600E}$ epitope. Vinculin was used as a loading control.

Figure S6. Visualization of structural variants and DNA copy number aberrations, Related to Figure 6.
A. The two genomic breakpoints in A375R that resulted in the establishment of a gene encoding $BRAF^{V600E/DK}$. **B.** The two genomic breakpoints in 888melDR that resulted in the establishment of a gene encoding $BRAF^{V600E/DK}$. Red arrows indicate the location of the breaks, the blue star indicates the genomic location where the breakpoint is located after the duplication of the BRAF kinase domain. **C.** Circos plots visualizing the structural variants **(**SV) and DNA copy number aberrations detected in parental cell line 888mel and double resistant cell line 888melDR. Blue indicates inter-chromosomal SVs, red intra-chromosomal SV. **D.** Circos plots visualizing the SV and DNA copy number aberrations detected in 888melDR but not in 888mel, both genome wide (top) and for the three chromosomes associated with the amplification on chromosome 7 which includes *BRAF* (bottom). **E.** Circos plot visualising the SVs and DNA copy number aberrations detected in resistant cell lines A375R. **F.** Read count data for A375R for the *BRAF* locus. Each dot represents the average number (log_2) of reads per 5kb.

Figure S7. Mass Spectrometry Identification of $BRAF^{V600E/DK}$ protein, Related to Figure 6.
A. SDS-PAGE showing the result of the IP on the parental cell line 888mel and resistant cell line 888melDR. Blot shows input before IP (input), result after IP (IP) and left-over in the buffer (after IP)

B. Tryptic digest of the suspected $BRAF^{V600E/DK}$ gel band was analysed by LC-MS/MS. Sequence coverage of the predicted protein sequence was around 50%, with the protein sequence covered by identified peptides indicated in green. **C.** The covered sequence included the unique $BRAF^{V600E/DK}$ fusion peptide, unambiguously demonstrating duplication of the BRAF kinase domain and confirming the protein sequence predicted by the RNA-sequencing data.

Table S1. Success rate PDX platform, Related to Figure 1

Tumor samples	Number	Xenografted	Cell lines derived of PDX
$BRAF^{V600E/K}$	86	73 (85%)	21 (29%)
$NRAS^{Q61}$	10	10 (100%)	3 (30%)
$BRAF^{WT}NRAS^{WT}$	7	6 (85%)	3 (50%)
Total	103	89 (86%)	27 (30%)
Whole exome sequencing		19	
360-cancer gene panel		47	

Table S2. Tumor percentage of matched PDX pairs, Related to Figure 2

PDX	Tumor cells (%)	Tumor stroma (%)	Necrosis/ degeneration/ hemorrhage (%)
M005.X1	70	25	5
M005R.X1	60	35	5
M009.X1	99	1	0
M009R.X1	87	3	10
M019.X1	80	5	15
M019R.X1	95	5	0
M026.X1	40	1	59
M026R.X1	15	1	84
M029.X1	98	1	1
M029R.X1	84	1	15
M048.X1	90	10	0
M048R1.X1	90	5	5
M048R2.X1	80	3	17

Table S3. Mutations detected in PDX panel after targeted sequencing, Related to Figure 4
This table is available as an excel file separately uploaded with this submission.

Table S4. Unmatched PDX samples, Related to Figure 5

Tumor samples	Pre-treatment	Post-treatment	Total
$BRAF^{V600E}$	19	19	38
$NRAS^{Q61}$	2	1	3
$BRAF^{WT}NRAS^{WT}$	2		2
TIL therapy		5	5
Total			47

Table S5. Previously known resistance mechanisms present in PDX derived from vemurafenib-resistant patients, Related to Figure 5

Sample	Best Clinical response	Duration	Resistance mechanism	Reference
M001R.X1	PR	10 months	$BRAF^{L505H}$	(Choi et al., 2014; Wagenaar et al., 2014)
M004R.X1	PR	4 months	BRAF splicing	(Poulikakos et al., 2011)
M006R.X1	PR	4 months	$NRAS^{Q61K}$ BRAF splicing	(Nazarian et al., 2010; Poulikakos et al., 2011)
M010R.X1	SD	6 months	MITF amplification	(Van Allen et al., 2014)
M013R.X1	PR	6 months	$PIK3CA^{E545K}$ Loss of PTEN	(Paraiso et al., 2011; Shi et al., 2014)
M014R.X1	PR	12 months		
M031R.X1	PR	7 months	BRAF splicing	(Poulikakos et al., 2011)
M033R.X1	CR	6 months		
M034R.X1	PR	10 months		
M039R.X1	PR	10 months	BRAF splicing Loss of PTEN	(Paraiso et al., 2011; Poulikakos et al., 2011)
M042R.X1	PR	8 months	BRAF amplification	(Thakur et al., 2013)
M044R.X1	SD	10 months	MET overexpression	(Vergani et al., 2011)
M054R.X1	SD	12 months		
M056R.X1	MR	6 months	$MAP2K1^{E203K}$ BRAF splicing EGFR overexpression	(Nikolaev et al., 2012; Poulikakos et al., 2011; Prahallad et al., 2012)
M060R.X1	PR	10 months	$PIK3CA^{E545K}$ EGFR overexpression	(Prahallad et al., 2012; Shi et al., 2014)
M061R.X1	PR	10 months	EGFR overexpression	(Prahallad et al., 2012)
M062R.X1	PR	12 months	$BRAF^{L505H}$ MITF amplification	(Choi et al., 2014; Van Allen et al., 2014; Wagenaar et al., 2014)
M063R.X1	SD	4 months		
M074R.X1	PD	2 months		

PR = partial response, SD = stable disease, CR = complete response, MR = mixed response

Table S6. Sample identifiers and number of supporting reads from RNAseq for BRAF$^{V600E/DK}$ detected in an independent dataset, Related to Figure 6.

GEO ID	Patient ID	Treatment	# reads
GSM1588858	Pt3-DP1	BRAFi	2
GSM1588860	Pt3-DP3	BRAFi	7
GSM1588901	Pt20-DDP1	BRAFi+MEKi	45
GSM1588902	Pt20-DP1	BRAFi	12

Table S7. Primers and hairpins, Related to Figure 2, 6 and 7.

Primer name	Sequence
$NRAS^{Q61K}$-F	5'- GATTCTTACAGAAAACAAGTG-3'
$NRAS^{Q61K}$-R	5'- ATGACTTGCTATTATTGATGG-3'
$AKT3^{L51R}$-F	5'- TGGAGGCCAAGATACTTCCTT-3'
$AKT3^{L51R}$-R	5'- ATGTGTTTGGCTTTGGTCGT-3'
$AKT3^{L51R}$-seq	5'- GGCTCATTCATAGGATATAA-3'
LINE-F	5'- AAAGCCGCTCAACTACATGG-3'
LINE-R	5'- TGCTTTGAATGCGTCCCAGAG-3'
CRAF-F	5'- CAACTGATTGCACTGACTGCCAAC-3'
CRAF-R	5'- CCAGCTTTCTACTCACCGCACAAC-3'
BRAF-F	5'- CAAGTCACCACAAAAACCTATCGT-3'
BRAF-R	5'- AACTGACTCACCACTGTCCTCTGTT-3'
BRAF-exon 18-F	5'-ATTCTCGCCTCTATTGAGCT-3'
BRAF-exon 10-R	5'- AAGGCTTTCACGTTAGTTAG-3'
BRAF-exon 9-F	5'-AGACCAAGGATTTCGTGGTGA-3'
BRAF-exon 10-R	5'- AGTGAGCCAGGTAATGAGGCA-3'
$BRAF^{V600E/DK}$-breakpoint-A375R-F	5'-GCCAGGCTCAAAATCAAACA-3'
$BRAF^{V600E/DK}$-breakpoint-A375R-R	5'-TGCACAGGCATTCATAGAAA-3'
$BRAF^{V600E/DK}$-breakpoint-888melDR-F	5'-TTTTTTTTTGAGATGGAGCTTGCTC-3'
$BRAF^{V600E/DK}$-breakpoint-888melDR-R	5'-GACTAAGTAATTGAAACAAAAG-3'
$BRAF^{V600E/DK}$-F-XbaI	5'- GGGTCTAGAATGGCCGGCTCTCGGTTATAAGATG-3'
$BRAF^{V600E/DK}$-R-SwaI	5'-GGGATTTAAATTCAGTGGACAGGAAACGCACCAT-3'
$BRAF^{V600E/DK}$ shRNA#1-F:	5'-CCGGgatatggatcaaccacaggtCTCGAGacctgtggttgatccatatccTTTTTG-3'
$BRAF^{V600E/DK}$ shRNA#1-R	5'-AATTCAAAAAggatatggatcaaccacaggtCTCGAGacctgtggttgatccatatcc-3'
$BRAF^{V600E/DK}$ shRNA#2-F	5'-CCGGtatggatcaaccacaggtttgCTCGAGcaaacctgtggttgatccataTTTTTG-3'
$BRAF^{V600E/DK}$ shRNA#2-R	5'-AATTCAAAAAtatggatcaaccacaggtttgCTCGAGcaaacctgtggttgatccata-3'

Supplemental Experimental Procedures

Response data patients
CT scans were used to determine the size of independent lesions at different time points. The size of a lesion was defined as the longest in plane diameter (in mm), measured manually by the tool provided in the Inter PACS Viewing & sharing System. For consistency, every lesion was measured by the same person on all subsequent CT scans. To ensure objectivity, this person was blinded for any other data of the patient in question.

DNA isolation
DNA was isolated from granulocytes derived from peripheral blood and tumor fragments using the DNA Easy Blood & Tissue Kit (Qiagen) according to manufacturer's protocol. DNA content was measured using Picogreen (P7581) according to manufacturer's protocol.

ArrayCGH analysis
DNA samples and normal genomic DNA (female, G1521, Promega) were labeled with CGH labeling kit for BAC Arrays (Enzo Life Sciences) according to manufacturer's protocol. After labeling, the samples were hybridized on a Nimblegen array (090527_HG18_WG_CGH_v3.1_HX12,_GEO platform ID: GPL17641). Image acquisition of the Nimblegen arrays was performed using the Agilent DNA Microarray Scanner (Model G2505B, Serial number US22502518) and image analysis was performed using Nimblescan software version 2.6 (Roche Nimblegen). Segmentation of all copy number profiles was calculated using circular binary segmentation (CBS) as implemented in the R-package CGHcall 2.22.0 (van de Wiel et al., 2011).

Whole Genome Sequencing of cell lines
DNA of parental 888mel, dabrafenib and trametinib double resistant 888mel (888melDR) and PLX4720-resistant A375 (A375R) was isolated as described above. Sequencing with 151bp paired-end reads of sequence libraries was performed on the Illumina X10 analyzer. Reads were mapped to the Sanger human reference (hg19) and BAM files were binary compressed, sorted and indexed by SAMtools (samtools view, sort and index tools), duplicated reads were removed by Picard (with MarkDuplicates) and base quality score recalibration and local realignment around indels followed the recommended workflow of the GATK toolkit (RealignerTargetCreator, IndelRealigner, BaseRecalibrator and PrintReads). Sequencing data has been made available through the European Genome-phenome Archive (EGA; http://www.ebi.ac.uk/ega/home; accession number EGAS00001001304).

Whole exome sequencing of matched PDX
DNA of 21 PDX samples with matching reference (blood) was isolated as described above and subjected to whole exome sequencing. Exome enrichment was performed using the Agilent SureSelect Human Exon Kit 50Mb capture set (Agilent, G3362). Sequencing with 75bp paired-end reads of targeted-enrichment libraries was performed on an Illumina HiSeq 2000 analyzer. Reads were mapped by bwa 0-7.5 with default settings to the human reference (hg19) and mouse reference (mm10), the latter for later removal of reads from mouse origin, as described below. BAM files were processed using Picard [1.101], SAMtools [0.1.18] and the Genome Analysis ToolKit (GATK) release 2.7-4. BAM files were binary compressed, sorted and indexed by SAMtools (samtools view, sort and index tools), duplicated reads were removed by Picard (with MarkDuplicates) and base quality score recalibration and local realignment around indels followed the recommended workflow of the GATK toolkit (RealignerTargetCreator, IndelRealigner, BaseRecalibrator and PrintReads). BAM files were further processed by removing reads that originate from mouse with XenofilteR release version 1.3 (https://github.com/PeeperLab/XenofilteR, Kluin and Krijgsman, manuscript in preparation. For each read-pair we summed the number of soft-clips, mismatches and inserts, both for mapping against the human as well as the mouse reference. The derived scores were used to classify reads as either mouse or human. Only reads with a lower score in human compared to mapping to mouse were retained in the final bam files.

Variants were called by GATK 2.7-4 using the 'UnifiedGenotyper' with default settings except for "-minIndelFrac" which was set to 10%. Annotation of the vcf files was performed with ANNOVAR (release 2014, October) (http://www.openbioinformatics.org/annovar/). All variants detected in the germ-line (blood) samples with a Variant Allele Frequency (VAF) over 5% were excluded from further analysis. Variants were further filtered: minimum VAF of 5% in at least one of the samples; a

minimum of 10x coverage in a least one of the samples; variant positions must not be listed as a single nucleotide polymorphism (SNP) in the 1000 Genome project except when present in COSMIC; Variant position must be annotated as exonic by RefSeq (Release 45); synonymous/non-synonymous calls were made and the synonymous excluded from further analysis. All filtering was performed with R 3.1.1 using in-house parsers. Sequencing data has been made available through the European Genome-phenome Archive (EGA; http://www.ebi.ac.uk/ega/home; accession number EGAS00001000415 and EGAS00001000617).

Targeted sequencing of unmatched PDX

DNA of 48 PDX samples was isolated as described above and subjected to targeted sequencing of 360 established and putative cancer-related genes using custom-made bait set (Agilent Technologies) for target enrichment. Paired-end sequencing was performed on Illumina HiSeq 2000 or 2500 analyzers. The raw sequence reads were processed similar to the WES data with the difference that no blood reference was available. The observed variants were referenced with polymorphisms catalogued by the 1000 genomes project (1000 Genomes Project Consortium et al., 2010) to remove known germline variants. Sequencing data has been made available through the European Genome-phenome Archive (EGA; http://www.ebi.ac.uk/ega/home; dataset ID: study ID: EGAS00001000655)

DNA copy number profiles

BAM files from targeted sequencing and whole exome sequencing were analyzed for DNA copy number aberrations by CopywriteR (Kuilman et al., 2015). DNA copy number profiles of matched PDX samples, analyzed with whole exome sequencing, were generated with 20kb bins, resulting in ~137K data points evenly distributed over the genome. Log_2ratios were calculated for tumor samples versus reference (blood) sample.

DNA copy number profiles of unmatched PDX samples, analyzed with targeted sequencing, were generated with 100kb bins, resulting in ~25K data points evenly distributed over the genome. Log_2 values were calculated based on tumor samples without a reference as described in (Kuilman et al., 2015).

DNA copy number profiles of cell lines 888mel, 888melDR and A375R, analyzed with WGS, were generated with 5kb bins evenly distributed over the genome. The resulting read count data was normalized similar to the WES data by loess normalization based on GC-content and mappability. Differences in DNA copy number between parental 888mel and 888melDR were assessed by subtracting the log2 of the read count of 888mel from the log2 read count of 888melDR. All normalized profiles were further analyzed by circular binary segmentation (CBS) (Venkatraman and Olshen, 2007).

Structural variation in WGS

Structural variations in cell lines 888mel, 888melDR and A375R were assessed directly on the WGS bam files with breakdancer (Chen et al., 2009). Only structural variants with a confidence score of 99 and a minimum of 10 supporting reads were used for the analysis. In addition, the minimum length between 2 intra-chromosomal breakpoints was set to 1mb. To assess the difference between 888mel and 888melDR all structural variants present in 888mel were removed from the list of structural variations in 888melDR. Circos plots were generated with (Zhang et al., 2015) using the DNA copy number data as described above and the filtered list of structural variations.

RNA isolation and sequencing

RNA isolated by Trizol, according to manufacturers protocol, from Fresh-Frozen (FF) PDX samples and Formalin-Fixed, Paraffin-Embedded (FFPE) patient archival tissue was sequenced with 50bp single-end sequencing on an Illumina HiSeq2000. Read counts per gene were quantified using HTSeq version 0.5.4. Read mapping was performed using TopHat version 2.0.9 with the NCBI Build 37 reference genome. Read counts were transformed by applying a variance stabilization with DESeq (1.12.1). In DESeq the dispersion estimate estimateDispersions had parameters: *method* 'per-condition' and *fitType* 'local' and for null model evaluation with no replicates *method* 'blind', and *sharingMode* 'fit-only'. Gene expression differences between PDX (FF) and patient (FFPE) read count data were observed by cluster analysis. Of the 21.467 genes in the initial analysis 1399 genes were differentially expressed (FDR<0.2) between the PDX and patient samples. After removal of these 1,399 genes the samples were clustered again with the remaining 20,068 genes. Heatmaps were generated with gplots

(2.12.1) as available through Bioconductor. Analysis was performed, and plots were made using the statistical programming language R (v 3.0.2).

RNA isolated from 4 FF PDX samples (M010R.X1, M033R.X1, M063R.X1 and M048R2.X1) was sequenced with 65bp paired-end sequencing on an Illumina HiSeq 2500. Discordant read pairs with both reads mapping within in BRAF were identified from the Tophat 'fusions.out' file and visually inspected in IGV to verify the breakpoints associated with the $BRAF^{V600E}$ kinase duplication. Both RNA sequence data sets are available through accession number GSE73738.

Raw data (fastq) from an independent dataset (Hugo et al., 2015) were downloaded from NCBI's Sequence Read Archive (SRA, SRP052740). Read mapping was performed using TopHat version 2.0.9 with the NCBI Build 38 reference genome. Discordant read pairs with both reads mapping within in BRAF were identified from the Tophat 'fusions.out' file and visually inspected in IGV to verify the breakpoints associated with the $BRAF^{V600E}$ kinase duplication.

FISH

Preparation of metaphase chromosome spread from parental Mel888 and double resistance Mel888 was performed as previously described (van Steensel et al., 1998).Two-color metaphase FISH was performed using chromosome 7 centromere probe (Chr7 CEP GR, G100527G-8, Agilent) and BRAF probe (7q34 BRAF-CN RD, G100368R-8, Agilent) according to the manufacturer's protocol.

Mass-spectrometry analysis of $BRAF^{V600E/DK}$

Mouse-anti-B-RAF (F7, Santa Cruz) antibodies were cross-linked to Dynabeads protein G (Cat #:10003D) according to the manufacturer's instruction. Cell lysates were incubated with these Dynabeads for 2h at 4°C. After washing 5 times with immunoprecipitation (IP) buffer (50 mM Tris-Cl, pH 8.0, 150 mM NaCl, 1.0% NP-40), elution was performed by boiling in NaPAGE LDS sample buffer (NP0008, Novex) and then processed for SDS-PAGE. Following staining of the SDS-PAGE gel with GelCode Blue stain (Pierce), the $BRAF^{V600E/DK}$ protein band was excised, proteins in the gel plug were reduced with DTT (1 hr at 60^0C) and subsequently alkylated using iodoacetamide (30 min at RT in the dark). In-gel digestion with 3ng/uL trypsin (Gold, Mass Spectrometry Grade, Promega) in 50 mM ammonium bicarbonate (pH 8.5) was performed overnight at 37 ^{o}C. After digestion, peptides were extracted with acetonitrile and dried down in a speed vacuum centrifuge. Prior to mass spectrometry analysis, the peptides were reconstituted in 10% formic acid.

Peptides were separated using the Proxeon nLC 1000 system (Thermo Scientific, Bremen) fitted with a trapping (ReproSil-Pur 120 C18-AQ 3µm (Dr. Maisch GmbH, Ammerbuch, Germany); 100 µm x 30 mm) and an analytical column (ReproSil-Pur 120 C18-AQ 2.4 µm (Dr. Maisch GmbH); 75 µm x 500 mm), both packed in-house. The outlet of the analytical column was coupled directly to a Thermo Orbitrap Fusion hybrid mass spectrometer (Q-OT-qIT, Thermo Scientific) using the Proxeon nanoflex source. Nanospray was achieved using a distally coated fused silica tip emitter (generated in-house, o.d. 375 µm, i.d. 20 µm) operated at 2.1 kV. Solvent A was 0.1% formic acid/water and solvent B was 0.1% formic acid/ACN. An aliquot (25%) of the in-gel digest was eluted from the analytical column at a constant flow rate of 250 nl/min in a 35-min gradient, containing a linear increase from 7% to 25% solvent B, followed by wash at 80% solvent B. Survey scans of peptide precursors from m/z 375-1500 were performed at 120K resolution with a 4 x 10^5 ion count target. Tandem MS was performed by quadrupole isolation at 1.6 Th, followed by HCD fragmentation with normalized collision energy of 33 and ion trap MS^2 fragment detection. The MS^2 ion count target was set to 10^4 and the max injection time was set to 50 ms. Only precursors with charge state 2-6 were sampled for MS^2. Monoisotopic precursor selection was turned on; the dynamic exclusion duration was set to 30s with a 10 ppm tolerance around the selected precursor and its isotopes. The instrument was run in top speed mode with 3 s cycles.

Raw data files were processed using Proteome Discoverer (version 1.4.1.14, Thermo Fisher Scientific). MS^2 spectra were searched against a custom database containing contaminants and the predicted sequence of the $BRAF^{V600E/DK}$ protein using Mascot (version 2.4.1, Matrix Science, UK). Carbamidomethylation of cysteines was set as fixed modification and oxidation of methionine was set as a variable modification. Trypsin was specified as enzyme and up to two miscleavages were allowed. Data filtering was performed using percolator, resulting in 1% false discovery rate (FDR), and peptide ion score >20.

Supplemental References

1000 Genomes Project Consortium, Abecasis, G.R., Altshuler, D., Auton, A., Brooks, L.D., Durbin, R.M., Gibbs, R.A., Hurles, M.E., and McVean, G.A. (2010). A map of human genome variation from population-scale sequencing. Nature *467*, 1061–1073.

Chen, K., Wallis, J.W., McLellan, M.D., Larson, D.E., Kalicki, J.M., Pohl, C.S., McGrath, S.D., Wendl, M.C., Zhang, Q., Locke, D.P., et al. (2009). BreakDancer: an algorithm for high-resolution mapping of genomic structural variation. Nat Meth *6*, 677–681.

Choi, J., Landrette, S.F., Wang, T., Evans, P., Bacchiocchi, A., Bjornson, R., Cheng, E., Stiegler, A.L., Gathiaka, S., Acevedo, O., et al. (2014). Identification of PLX4032-resistance mechanisms and implications for novel RAF inhibitors. Pigment Cell & Melanoma Research *27*, 253–262.

Hugo, W., Shi, H., Sun, L., Piva, M., Song, C., Kong, X., Moriceau, G., Hong, A., Dahlman, K.B., Johnson, D.B., et al. (2015). Non-genomic and Immune Evolution of Melanoma Acquiring MAPKi Resistance. Cell *162*, 1271–1285.

Kuilman, T., Velds, A., Kemper, K., Ranzani, M., Bombardelli, L., Hoogstraat, M., Nevedomskaya, E., Xu, G., de Ruiter, J., Lolkema, M.P., et al. (2015). CopywriteR: DNA copy number detection from off-target sequence data. Genome Biology *16*, R163.

Nazarian, R., Shi, H., Wang, Q., Kong, X., Koya, R.C., Lee, H., Chen, Z., Lee, M.-K., Attar, N., Sazegar, H., et al. (2010). Melanomas acquire resistance to B-RAF(V600E) inhibition by RTK or N-RAS upregulation. Nature *468*, 973–977.

Nikolaev, S.I., Rimoldi, D., Iseli, C., Valsesia, A., Robyr, D., Gehrig, C., Harshman, K., Guipponi, M., Bukach, O., Zoete, V., et al. (2012). Exome sequencing identifies recurrent somatic MAP2K1 and MAP2K2 mutations in melanoma. Nature Genetics *44*, 133–139.

Paraiso, K.H.T., Xiang, Y., Rebecca, V.W., Abel, E.V., Chen, Y.A., Munko, A.C., Wood, E., Fedorenko, I.V., Sondak, V.K., Anderson, A.R.A., et al. (2011). PTEN loss confers BRAF inhibitor resistance to melanoma cells through the suppression of BIM expression. Cancer Res. *71*, 2750–2760.

Possik, P.A., Müller, J., Gerlach, C., Kenski, J.C.N., Huang, X., Shahrabi, A., Krijgsman, O., Song, J.-Y., Smit, M.A., Gerritsen, B., et al. (2014). Parallel in vivo and in vitro melanoma RNAi dropout screens reveal synthetic lethality between hypoxia and DNA damage response inhibition. Cell Rep *9*, 1375–1386.

Poulikakos, P.I., Persaud, Y., Janakiraman, M., Kong, X., Ng, C., Moriceau, G., Shi, H., Atefi, M., Titz, B., Gabay, M.T., et al. (2011). RAF inhibitor resistance is mediated by dimerization of aberrantly spliced BRAF(V600E). Nature *480*, 387–390.

Prahallad, A., Sun, C., Huang, S., Di Nicolantonio, F., Salazar, R., Zecchin, D., Beijersbergen, R.L., Bardelli, A., and Bernards, R. (2012). Unresponsiveness of colon cancer to BRAF(V600E) inhibition through feedback activation of EGFR. Nature *483*, 100–103.

Shi, H., Hong, A., Kong, X., Koya, R.C., Song, C., Moriceau, G., Hugo, W., Yu, C.C., Ng, C., Chodon, T., et al. (2014). A novel AKT1 mutant amplifies an adaptive melanoma response to BRAF inhibition. Cancer Discovery *4*, 69–79.

Thakur, Das, M., Salangsang, F., Landman, A.S., Sellers, W.R., Pryer, N.K., Levesque, M.P., Dummer, R., McMahon, M., and Stuart, D.D. (2013). Modelling vemurafenib resistance in melanoma reveals a strategy to forestall drug resistance. Nature *494*, 251–255.

Van Allen, E.M., Wagle, N., Sucker, A., Treacy, D.J., Johannessen, C.M., Goetz, E.M., Place, C.S., Taylor-Weiner, A., Whittaker, S., Kryukov, G.V., et al. (2014). The genetic landscape of clinical resistance to RAF inhibition in metastatic melanoma. Cancer Discovery *4*, 94–109.

van de Wiel, M.A., Picard, F., van Wieringen, W.N., and Ylstra, B. (2011). Preprocessing and

downstream analysis of microarray DNA copy number profiles. Brief. Bioinformatics *12*, 10–21.

van Steensel, B., Smogorzewska, A., and de Lange, T. (1998). TRF2 protects human telomeres from end-to-end fusions. Cell *92*, 401–413.

Venkatraman, E.S., and Olshen, A.B. (2007). A faster circular binary segmentation algorithm for the analysis of array CGH data. Bioinformatics *23*, 657–663.

Vergani, E., Vallacchi, V., Frigerio, S., Deho, P., Mondellini, P., Perego, P., Cassinelli, G., Lanzi, C., Testi, M.A., Rivoltini, L., et al. (2011). Identification of MET and SRC activation in melanoma cell lines showing primary resistance to PLX4032. Neoplasia *13*, 1132–1142.

Vredeveld, L.C.W., Possik, P.A., Smit, M.A., Meissl, K., Michaloglou, C., Horlings, H.M., Ajouaou, A., Kortman, P.C., Dankort, D., McMahon, M., et al. (2012). Abrogation of BRAFV600E-induced senescence by PI3K pathway activation contributes to melanomagenesis. Genes & Development *26*, 1055–1069.

Wagenaar, T.R., Ma, L., Roscoe, B., Park, S.M., Bolon, D.N., and Green, M.R. (2014). Resistance to vemurafenib resulting from a novel mutation in the BRAFV600E kinase domain. Pigment Cell & Melanoma Research *27*, 124–133.

Zhang, L., Zhou, Y., Cheng, C., Cui, H., Cheng, L., Kong, P., Wang, J., Li, Y., Chen, W., Song, B., et al. (2015). Genomic analyses reveal mutational signatures and frequently altered genes in esophageal squamous cell carcinoma. Am. J. Hum. Genet. *96*, 597–611.